Microstructural Classification and Reconstruction of the Computational Geometry of Steamed Bread Using Descriptor-Based Approach

Clement Kehinde Ajani[1,2,3] · Zhiwei Zhu[1,2,3] · Da-Wen Sun[1,2,3,4]

Abstract

Microstructures affect the properties of food products; accurate and relatively less complex microstructural representations are thus needed for modelling of transport phenomena during food processing. Hence, the present study aimed at developing computational microstructures of steamed bread using descriptor-based approach. Relevant information was extracted from the scanning electron microscope (SEM) images of the steamed bread and evaluated using seven classifiers. For the automatic classification and using all descriptors, bagged trees ensembles (BTE) had the highest accuracy of 98.40%, while Gaussian Naïve Bayes was the least with 92.10% accuracy. In the "step forward" analysis, five descriptors had higher classification accuracy (98.80%) than all descriptors, implying that increase in descriptors might or might not increase classification accuracy. Microstructural validation revealed that the ellipse fitting method with a p value of 0.7984 for the area was found to be superior to the Voronoi method with a corresponding p value of 1.4554×10^{-5}, confirming that the ellipse developed microstructure was more suitable for microscale modelling of transport phenomena in steamed bread.

✉ Da-Wen Sun
dawen.sun@ucd.ie
http://www.ucd.ie/refrig
http://www.ucd.ie/sun

1   School of Food Science and Engineering, South China University of Technology, Guangzhou 510641, China

2   Guangzhou Higher Education Mega Centre, Academy of Contemporary Food Engineering, South China University of Technology, Guangzhou 510006, China

3   Engineering and Technological Research Centre of Guangdong Province on Intelligent Sensing and Process Control of Cold Chain Foods, and Guangdong Province Engineering Laboratory for Intelligent Cold Chain Logistics Equipment for Agricultural Products, Guangzhou Higher Education Mega Centre, Guangzhou 510006, China

4   Food Refrigeration and Computerized Food Technology (FRCFT), Agriculture and Food Science Centre, University College Dublin, National University of Ireland, Belfield, Dublin 4, Ireland

1 Introduction

Microstructures or structural features at the cellular level such as cells, cellular spaces, gas cells, solid matrices and their organization contribute to the quality attributes of food products such as texture, sensory, rheological property and shelf-life (Houska et al. 2005; Drummond et al. 2009; Abera et al. 2014). On the other hand, microstructural elements strongly affect the transport properties of food especially porous food products as transport of bound and free water through the various microstructural features takes place at this scale (Aguilera et al. 2000; Aguilera 2005). In addition, food processing affects the stability of the microstructure, which in turn affect food quality (Cheng and Sun 2007; Feng and Sun 2014).

Mathematical modelling is a valuable tool to understand and optimize food processes (Zhang and Sun 2005). In particular, modelling at the microstructural level is a key to comprehend the microscale chemical and physical phenomena, which are lumped together in macroscale modelling (Sun and Hu 2003; Wang and Sun 2003; Ajani et al. 2019). Moreover, the multiscale modelling paradigm has been recently employed in food material modelling (Rahman et al. 2018a). For achieving reliable modelling results, accurate microstructural representations are needed, which in turn require adequate microstructural information.

Bread is one of the most common staple foods in the world, and steamed bread is a popular Chinese staple, which is mostly made from plain flour, water and yeast with or without stuffing (Kou et al. 2019). Steam bread is a typical porous food product. The transport properties of bread significantly affect their freshness, colour, crispiness, water diffusivity, microstructural stability, sensorial, textural, rheological properties and staling during steaming and storage (Altamirano-fortoul et al. 2012; Drummond and Sun 2012). The structure of steam bread consists of an assemblage of microstructures with a large number of pores or gas cells heterogeneously distributed across the interconnected solid matrices (Aguilera 2005); therefore, steam bread is complex with multiscale fractal-like hierarchical structures (Ajani et al. 2020; Heertje 2014).

Both descriptor-based and correlation function-based approaches are reliable for the characterization, classification, reconstruction and modelling of food microstructures (Derossi et al. 2014, 2016; Sundararaghavan and Zabaras 2005; Xu et al. 2014a). Microstructural reconstruction generally involves two main steps: the extraction of representative information from the microstructural image, which can be either a descriptor-based approach or a correlation function-based approach and the generation of the virtual microstructure, which includes Voronoi tessellation algorithm, ellipse tessellation algorithm, etc.

Among the two approaches for information extraction, the descriptor-based approach shows its strengths including adequate microstructural representation with well-defined physical meaning, and lower reconstruction cost (Thomas et al. 2008; Xu et al. 2014a) and thus, plays an important role in reliable mathematical modelling and is often used as representative element volume (REV) to model food transport phenomena during processing at the microscale (McDonald and Sun 2000; Rahman et al. 2018b). Geometry descriptors are computational methods used to analyse, quantify and represent an image in quantitative image analysis (Prakash et al. 2011; Xu et al. 2014a). These descriptors can be quantified by mean or higher-order moments such as variance, kurtosis depending on the availability of sufficient descriptor sets (Xu et al. 2014b).

For the generation of the virtual microstructure, some researchers used the Voronoi tessellation algorithm for developing microstructures of apples in different cultivars

(Mebatsion et al. 2006a) and pome fruits (Abera et al. 2014), while others used ellipse tessellation algorithm for constructing the virtual microstructures of apples, onions, and conference pear tissues (Mebatsion et al. 2006b; Rahman et al. 2018b), showing better accuracy than the former. Both algorithms are descriptor based; however, in most cases, the use of the extracted geometrical descriptors in classifying and differentiating between the cells and intercellular spaces was not carried out, and the cells and intercellular spaces were randomly chosen in the developed microstructures, leading to low accuracies in modelling. Moreover, in some studies, only a single classifier was used in evaluating the sufficiency and sensitivity of the geometrical descriptors and detailed statistical evaluation of the prediction errors between the classes was not considered, resulting in a limited understanding of the discriminative power of the classifier. On the other hand, the application of both algorithms was mostly limited to the development of fruit microstructures, and no application has been found for foods such as bread. Although the microstructures of fruits are heterogeneous, which consist of cells, cell walls and intercellular spaces, their structural features and organization are different from those of bread. The bread microstructures primarily consist of pore or gas cell, laminae and networks of solid matrices which could be continuous or discontinuous, depending on the gas cell stability during processing (Sun and Wang 2006; Wang et al. 2011).

Due to the heterogeneous nature of food microstructures at the microscale, it is hard to differentiate their relevant features. Hitherto, only linear discriminant analysis (LDA) combined with relevant geometrical descriptors has been used as an automatic classifier for food microstructural features (Decost and Holm 2015; Pieczywek and Zdunek 2012; Rahman et al. 2018c), while the use of other relevant classifiers such as bagged trees ensembles (BTE) and Rusboosted trees ensembles (RTE), which could achieve better discrimination such as in the case of class imbalance (Tharwat et al. 2017), has not been investigated. Class imbalance exists when the samples in a class greatly outnumber those of the other classes in a dataset (Seiffert et al. 2010).

Although the connectivity of a 3D microstructure is greater than 2D counterpart, the latter is much easier to investigate, convenient to interpret, computationally economical, and has thus been mostly used for microscale and even multiscale modelling of food products with accurate predictions (Wang and Sun 2002a, b; Aregawi et al. 2014; Rahman et al. 2018b). Moreover, for practical industrial applications, morphological features in 3D images are often analysed using 2D projections and the developed 2D microstructures can be easily extended to 3D (Abera et al. 2014; Su and Yan 2020). Specifically, the fractal method is often used for bread analysis, assuming that the shapes are self-similar across different hierarchies and cross sections, thus making a 2D analysis sufficient (Liu and Scanlon 2003; Gonzales-Barron and Butler 2008; Zhang et al. 2013). In addition, the 2D microstructures developed in the current work could be used for microscale transport modelling and upscaled to 3D in the multiscale.

Presently, most microscale modelling of bakery products uses simplified homogenous or network models with no detailed geometrical features (Esveld et al. 2012). On the other hand, models with complex geometrical features often create singularity with results that are relatively hard to interpret (Rahman et al. 2018b), and there is thus a need to develop more accurate but simple REV for bread microstructures to modelling the microscale transport phenomena during processing. Therefore, in the current study, a descriptor-based approach for 2D reconstruction of steamed bread microstructures from microscopic images was developed. With the geometrical descriptors extracted from the microstructures, seven classifiers including LDA, BTE, Gaussian Naïve Bayes (GNB), fine tree (FT), quadrative support vector machine (QSVM), fine k-nearest neighbour (FKNN) and RTE were

compared for automatic classification of the pores and solid matrices. Statistical information from SEM images together with Voronoi and ellipse tessellation algorithms was utilized for generating the virtual microstructures of the steamed bread, and the developed microstructural models were validated against the original SEM images by comparing various geometrical features including perimeter, area, orientation, centroid, convex area, circularity, and eccentricity.

2 Experimental Methods

SEM imaging was used for the development of 2D microstructural computational geometry in the current study. SEM images provide clear and detailed information on food microstructures even at microscale resolution with little or no chemical treatments (Pieczywek and Zdunek 2012; Rahman et al. 2018c). For the morphological observation by SEM, freshly prepared whole steamed bread samples were randomly purchased from a local bakery shop (Guangzhou, China), which were freeze-dried for about 24 h to remove the moisture, and the dried samples were stored in a desiccator. To reveal the microstructures, two samples were cut into cubes of about $1 \times 1 \times 1$ cm from different cross sections and regions using a sharp cutter. The cut samples were firmly mounted on metal stubs using a double-sided tape, placed inside an automatic sputter coater and platinum-plated. The coated samples were then placed inside a high-resolution scanning electron microscope (Zeiss Merlin Field Emission SEM, Carl Zeiss NTS GmbH, Oberkochen, Germany). A total of 40 images were taken from different sections of the samples at an accelerating voltage of 5 kV and a magnification of 24. The 40 images with 400×400 pixels sizes (1 pixel $= 4.686$ µm) were identified by region of interest (ROI), and digitally analysed. The geometrical descriptors such as the area, circularity, eccentricity, orientation, and convex area, perimeter and centroid were then extracted from the 40 images.

3 Statistical Estimation and Theoretical Formulation

The geometric shape analysis can be done using the area-based or/and the boundary-based approach, and the choices are mostly based on the organization of the shapes (Thomas et al. 2008).

3.1 Geometrical Properties Estimation

Although geometrical property estimation approaches based on set theory are well adapted for estimating geometrical features, especially in the 3D (Schröder-Turk et al. 2013; McClure et al. 2018), Green's theorem is suitable for less complex 2D microstructural reconstruction with reasonable accuracy and was thus employed in the current work. The geometrical descriptors, which are the characteristics of pores or gas cells, were estimated using ellipse fitting based on Green's theorem (Mebatsion et al. 2006a; Mulchrone and Roy 2004). These geometric descriptors include surface area, circularity, eccentricity, convex area, perimeter, etc. Green's theorem is one of the fundamental theorems of vector calculus, which defines the relationship between the macroscopic circulation of a curve and the sum of the microscopic circulation inside the curve (Chalifour et al. 2017). The theorem can also be used for calculating the amount of work done on a force field, the flux and flow

on a vector field, the area of conics with line integral, etc. (Mebatsion et al. 2006a; Chalifour et al. 2017). Given a Cartesian plane with x and y representing the horizontal and vertical values of the coordinate pair, respectively, let C be a simple closed curve in the plane and F be the region bounded by C, and given two functions $D(x, y)$ and $E(x, y)$, having a boundary F, the differentiable functions can be expressed using Green's theorem as

$$\iint_C \left(\frac{\partial D}{\partial x} - \frac{\partial E}{\partial y} \right) \mathrm{d}x\mathrm{d}y = \int_F (D\mathrm{d}x + E\mathrm{d}y) \tag{1}$$

The area A, also known as the zeroth moment of inertia, can be calculated as

$$A = \iint_C \mathrm{d}x\mathrm{d}y \tag{2}$$

The application of Green's transformation to Eq. (2) in anticlockwise direction yields

$$A = \frac{1}{2} \sum_{k=1}^{n} x_{k-1}y_k - x_k y_{k-1} \tag{3}$$

where the number of points on the pores is taken as n. The first moment (σ_x) with x-direction preference, otherwise known as the centroid of a region, is calculated as

$$\sigma_x = \frac{1}{A} \iint_C x\mathrm{d}x\mathrm{d}y \tag{4}$$

The application of Green's transformation to Eq. (4) yields

$$\sigma_x = \frac{1}{6A} \sum_{k=1}^{n} \left(x_{k-1} - x_k \right) \left(x_{k-1}y_k - x_k y_{k-1} \right) \tag{5}$$

The first moment (σ_y) with y-direction preference is given as

$$\sigma_y = \frac{1}{A} \iint_C y\mathrm{d}x\mathrm{d}y \tag{6}$$

Similarly, the application of Green's transformation to Eq. (6) yields

$$\sigma_y = \frac{1}{6A} \sum_{k=1}^{n} (y_{k-1} - y_k)\left(x_{k-1}y_k - x_k y_{k-1} \right) \tag{7}$$

3.2 Calculation of Eccentricity and Orientation

The eccentricity (aspect ratio) and orientation were also calculated from the images using ellipse fitting. Given a specific region on a boundary, having a number of points n, the second moment of the area can be calculated over x, y, and xy plane, respectively, as follows

$$\sigma_{xx} = \iint_R y^2 \mathrm{d}x\mathrm{d}y \tag{8}$$

$$\sigma_{yy} = \iint_R x^2 \mathrm{d}x\mathrm{d}y \tag{9}$$

$$\sigma_{xy} = \iint_R xy\mathrm{d}x\mathrm{d}y \tag{10}$$

σ_{xx}, σ_{yy}, σ_{xy} are the second moments of area calculated over x, y, and xy plane, respectively. The application of Green's transformation to Eqs. (8)–(10) yields

$$\sigma_{xx} = \frac{1}{12A} \sum_{k=1}^{n} \left(y_k^2 + y_k y_{k+1} + y_{k+1}^2\right)\left(x_{k+1}y_k - x_k y_{k+1}\right) \tag{11}$$

$$\sigma_{yy} = \frac{1}{12A} \sum_{k=1}^{n} \left(x_k^2 + x_k x_{k+1} + x_{k+1}^2\right)\left(x_{k+1}y_k - x_k y_{k+1}\right) \tag{12}$$

$$\sigma_{xy} = \frac{1}{24A} \sum_{k=1}^{n} \left(2x_k y_k + x_k y_{k+1} + y_k x_{k+1} + 2x_{k+1}y_{k+1}\right)\left(x_{k+1}y_k - x_k y_{k+1}\right) \tag{13}$$

The orientation and eccentricity of the pores were calculated from the estimated central area moments in the 2D spatial domain as

$$\alpha = \frac{1}{2}\tan^{-1}\left(\frac{2\mu_{11}}{\mu_{02} - \mu_{20}}\right) \tag{14}$$

$$e = \frac{l_1}{l_2} \tag{15}$$

where α is the orientation, e is the eccentricity, the central moments μ_{11}, μ_{02}, and μ_{20} were defined from their respective centroids and area moments of the pores, l_1 and l_2 are the major and minor length axes of the pores, respectively.

The summation of the distance among adjacent data set on the pore boundaries was used to calculate the perimeter. Circularity was calculated using the relationship below

$$\text{Circularity} = \frac{4\pi \, \text{Pore area}}{(\text{Convex perimeter})^2} \tag{16}$$

The circularity (Eq. 16) index ranges from 1 to 0 with 1 representing the perfectly circular shape and 0 representing irregularly shaped objects, which departs from circularity.

3.3 Identification of Key Descriptors for Classifying Pores and Solid Matrices

In previous works, most microstructural descriptors used for evaluating microstructural features are randomly chosen without providing any information on the significance of each descriptor to the microstructural features or properties of interest (Mebatsion et al. 2006a, b). Moreover, with the availability of a large number of microstructure descriptors, representing the microstructural features quantitatively using a descriptor set that is sufficient and yet small enough to be tractable is challenging (Xu et al. 2014a). Hence, machine learning (ML) approaches can be used to automatically evaluate the descriptors-features relationship and for fast selection of most relevant descriptors (Xu et al. 2014a, 2014b). Besides, the ML approach could be used to automatically classify the respective features in the reconstructed microstructures when imported as REV during microscale modelling especially in the case of large data set (Rahman et al. 2018c).

In the current study, the significance of each descriptor for classifying bread microstructural features (pores and solid matrices) was investigated. A dataset containing 6496 features (pores and solid matrices) of the bread was extracted from all the 40 images, and 80% of the dataset was used for training and 20% for testing. Specifically, 6037 pores and 459 solid matrices were identified from the images. The different types of pores that can be found in a porous food structure include open, closed, and blind pores (McDonald and Sun 2001a, b; Halder et al. 2011); hence, for steamed bread microstructures, all the pores were classified as a class, and the solid matrices as another. Seven classifiers were used for the automatic classification of the two classes, and the geometrical descriptors were used for training in MATLAB. Detailed mathematical formulations of the classifiers, which include LDA, RTE, GNB, FT, QSVM, FKNN, and BTE can be found in the literature (Hastie et al. 2008; Richards and Xiuping 2013). The classifiers used in this study were selected based on the class imbalance nature of the dataset (i.e. 6037 pores and 459 solid matrices), and their superior performance as demonstrated in similar works (Pérez-Ortiz et al. 2016; Rahman et al. 2018c; Seiffert, et al. 2010). The discriminative ability of the best classifier was further evaluated using confusion matrix since it shows the relationship between the classifier outputs and the true ones, which could not be revealed using Wilk's (λ) (Novakovic et al. 2017; Pieczywek and Zdunek 2012; Rahman et al. 2018c). Furthermore, a "step forward" analysis was used to identify key descriptors for classifying the pores and solid matrices (Pieczywek and Zdunek 2012). The classification accuracy of each classifier was calculated using the equation below:

$$\text{Accuracy} = \frac{\text{TN} + \text{TP}}{\text{TN} + \text{TP} + \text{FN} + \text{FP}} \tag{17}$$

where TN, TP, FN, and FP are the true negatives, true positives, false negatives, and false positives, respectively.

3.4 Voronoi Tessellation (VT)

Given a set of sites, $S = \{s_i, ..., s_n\}$ in the 2D Euclidean plane, Voronoi territory ($V(s_i)$) of the sites can be given as the partitioning of the plane having all points close to S_i as to any other site, which can be mathematically defined as

$$V(s_{\mathrm{i}}) = \left\{ \left| s_{\mathrm{i}} - x \right| \leq \left| s_{\mathrm{j}} - x \right|, \forall j \neq i \right\} \tag{18}$$
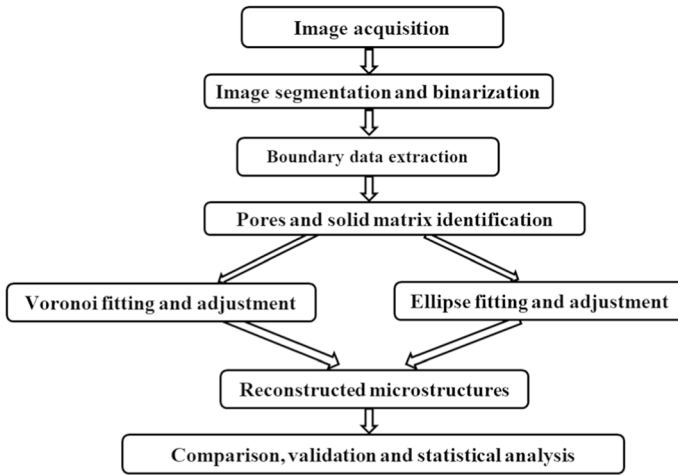
Fig. 1 Schematic diagram of reconstruction methods

The divisions into spaces by Voronoi tessellation are based on the number of points available. Also, the same number of points (centroids) in space in the actual cellular images was used for the random generation of the Voronoi diagrams. The Voronoi tessellation was developed using a MATLAB function called Voronoi. The schematic diagram of the microstructural reconstruction methods including the Voronoi and ellipse tessellation is shown in Fig. 1.

3.5 Ellipse Tessellation (ET)

The ellipse-fitting algorithm (Mebatsion et al. 2006b) was used for ellipse tessellation as given below

$$F(\text{x,y}) = ax^2 + bxy + cy^2 + dx + ey + f \tag{19}$$

where the ellipse coordinates and coefficients are denoted by (x, y), and $a, b, c, d, e, f,$ respectively. The algebraic distance between the two-point function is expressed by $F(x, y)$. Also, the constraint of the ellipse constraint is

$$b^2 - 4ac < 0 \tag{20}$$

Rewriting Eq. (19) yields

$$F(a;x) = ax \tag{21}$$

where $a = \left[a, b, c, d, e, f,\right]^T$ and $x = \left[x^2, xy, y^2, x, y, 1\right]^T$, respectively, with ^{T} representing the transposed vector.

Ellipse fitting of a general conic involves the minimization of algebraic distance over the set of data points in the least square sense. To fit the data point (x, y), the least square fitting can be used as follows (Rahman et al. 2018c)

$$\text{min mize} \sum_{i=1}^{N} F(x_i, y_i)^2 = \text{min imize} \sum_{i=1}^{N} (a, x_i)^2 \tag{22}$$

To ensure an ellipse-specificity of the solution, the vector a can be arbitrarily scaled, and the constraint equation given below is most appropriate

$$4ac - b^2 = 1 \tag{23}$$

Equation (23) can be expressed in matrix form as

$$a^T \begin{bmatrix} 0 & 0 & 2 & 0 & 0 & 0 \\ 0 & -1 & 0 & 0 & 0 & 0 \\ 2 & 0 & 0 & 0 & 0 & 0 \\ 0 & 0 & 0 & 0 & 0 & 0 \\ 0 & 0 & 0 & 0 & 0 & 0 \\ 0 & 0 & 0 & 0 & 0 & 0 \end{bmatrix} a = 1 \tag{24}$$

The pores centroid and area were numerically estimated using Eq. (22). The ellipse algorithm used the centroid, length of the major and minor axis, and orientation for the microstructural reconstruction ("Appendix"). Unlike plant-based food microstructures developments with no overlapping of cell sites (Mebatsion et al. 2006b; Rahman et al. 2018a), the ellipses representing the pores were directly fitted with most overlapping, since most bread structures are predominantly open pores with few closed pores, which also allows for easy network flow during transport modelling (Wang et al. 2011; Esveld et al. 2012). In addition, an ellipse was developed from a centroid as long as the data points belong to it; otherwise, the data points were used for other pores. For steamed bread, the gluten–starch solid matrices are mostly connected with irregular shapes; hence, the residual points were used to develop them. The above algorithm was implemented using MATLAB codes and terminated after all the data points in the microscopic images were calculated.

3.6 Image Processing

The post-processing of the images acquired from SEM was carried out in MATLAB (2019b, MathWorks, Natick, USA). The flowchart of the image processing is outlined in Fig. 1, including watershed segmentation, binarization, geometrical descriptor extraction, etc. The images were first segmented involving the discretization of the acquired images into different parts. The image intensities were used for marking discrete parts or regions from the background, and for more accurate pore boundary extraction, the watershed algorithm was used for segmentation (Brosnan and Sun 2002; Ng et al. 2006). Additionally, the points used for the watershed segmentation were obtained using the Pwdist function in MATLAB. From the grayscale images, the boundaries of the solid matrices and the pores were clearly distinct so that binarization based on a carefully selected threshold obtained by trial and error was sufficient enough to segment the pores from the solid matrices. However, the resulting image from the binarization process featured some noise, which was characterized by a typical salt and pepper noise. This noise was removed using the median filter. The extracted data were used for the reconstruction of the images with the ellipse and Voronoi algorithms. The reconstruction algorithms were selected due to their reputation for developing food microstructures with good accuracies (Abera et al. 2014; Rahman et al. 2018c). Moreover, the reconstructed microstructures were imported as a computational

domain into COMSOL Multiphysics (v.5.5., COMSOL AB, Stockholm, Sweden) and meshed.

3.7 Statistical Validation and Analysis

The accuracy of the reconstructed microstructures was evaluated by comparison with the original microstructures using Kolmogorov–Smirnov (K–S) with a 5% level of significance, and all statistical analysis was carried out using MATLAB.

4 Result and Discussion

4.1 Steamed Bread Microstructural Features

To show the distributions of the bread microstructural features (pore and solid matrix) analysed in this study, two samples were randomly selected from the 40 images (Fig. 2). Boxplots were drawn to reveal the distributions of steamed bread microstructural features as shown in Fig. 3, and each plot consists of mean, minimum value, maximum value, upper and lower quartile and spacing between box lines. Generally, for the two samples presented, the solid matrices had higher mean values than the pores in terms of area, perimeter and convex area. For example, for sample 1, the mean areas of the pores and solid matrices were 1737 μm^2 and 17,065 μm^2, respectively, while for sample 2, those were 1031 μm^2 and 1138 μm^2, respectively, as shown in Fig. 3a and b. The marked difference between the mean areas of the solid matrices for both samples was due to their distribution as shown in Fig. 2. For sample 1, the mean circularities of the pores and solid matrices were 0.6587 and 0.2319, respectively, while for sample 2, those were 0.6233 and 0.5772, respectively, as shown in Fig. 3c and d. It can be inferred from the mean circularities and 2D pictorial images of the microstructures that the pores were more circular than solid matrices, as such, during reconstruction, only the pores were fitted while the residual data points were taken as solid matrices.

Orientation is also an important descriptor used to describe microstructural features (Pieczywek et al. 2011). For samples 1, the mean orientations of the pores and solid matrices were 43.4173 and 30.9401, respectively, while for sample 2, those were 44.9162 and 28.7213, respectively, as shown in Fig. 3e and f.

Therefore, descriptors such as areas, perimeter, convex area, circularity and orientation are important for classifying the pores and solid matrices, since there was consistent variation in the mean values between both classes, they could thus be used to automatically classify microstructural features, and to reconstruct steamed bread microstructures which serve as REV for microscale transport modelling. The mean eccentricities for both samples did not follow any trend; for example, the mean eccentricity of the pores was higher than that of the solid matrices for sample 1, and vice versa for sample 2 as shown in Fig. 3g and h, indicating that eccentricity might not be an important descriptor for classifying the pores and solid matrices.

4.2 Identification of Key Descriptors for Pores and Solid Matrix Classification

Although the descriptor's mean value across bread microstructures provided some insights on potential descriptors for feature classification as discussed previously, it does not reveal
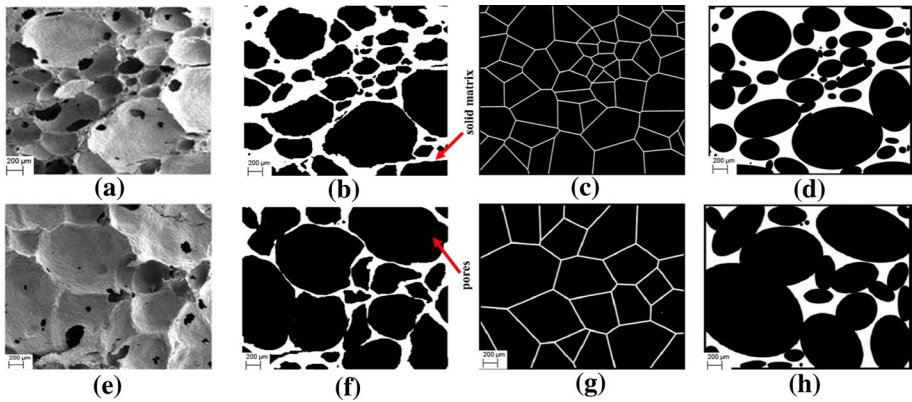
Fig. 2 **a** Raw SEM image for sample 1, **b** denoised, segmented and binary image for sample 1 **c** Voronoi generated microstructure for sample 1, **d** ellipse generated microstructure for sample 1, **e** raw SEM image for sample 2, **f** denoised, segmented and binary image for sample 2, **g** Voronoi generated microstructure for sample 2, **h** ellipse generated microstructure for sample 2
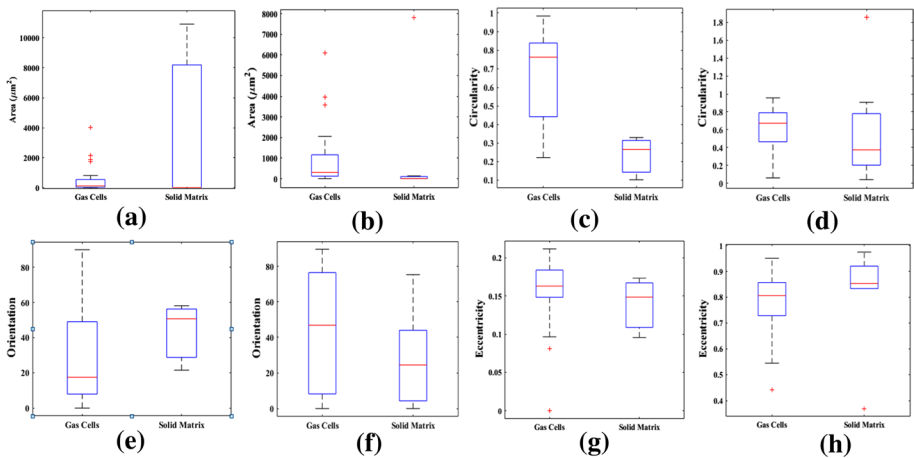
Fig. 3 Area distribution of pores and solid matrix for **a** sample 1 and **b** sample 2, circularity distribution of pores and solid matrix for **c** sample 1 and **d** sample 2, orientation distribution of pores and solid matrix for **e** sample 1 and **f** sample 2, eccentricity distribution of pores and solid matrix for **g** sample 1 and **h** sample 2

their significance. The classification accuracies of the seven classifiers using all and individual geometrical descriptors are presented in Table 1. For all the descriptors, the most performed classifier was BTE with 98.40% accuracy, while the least performed was GNB with 92.10% accuracy. However, in some other studies involving the classification of fruit microstructures, LDA was adopted as the most suitable classifier (Pieczywek and Zdunek 2012; Rahman et al. 2018c). This might be attributed to the differences between bread and fruit microstructures, and specific ability of the respective classifiers in handling the microstructural features (Pérez-Ortiz et al. 2016). Furthermore, the average accuracy was 94.61% for all classifiers, and the geometrical features used were thus sufficient to classify the pores and solid matrices (Decost and Holm 2015). In addition, the accuracies of most classifiers with all descriptors used were higher than those obtained using individual

Table 1 Results of binary classification between the pores and solid matrices using seven classifiers

Classifiers	Samples accuracy							
	All descriptors (%)	Area (%)	Centroid (%)	Orientation (%)	Perimeter (%)	Eccentricity (%)	Convex area (%)	Circularity (%)
FT	97.10	94.10	91.00	93.50	94.50	94.90	93.60	97.1
LDA	93.50	93.10	92.90	92.90	93.30	92.90	93.30	93.00
GNB	92.10	92.50	92.90	92.10	92.70	92.90	92.60	93.00
QSVM	95.20	93.00	92.90	80.10	74.40	43.80	58.80	7.90
FKNN	92.70	94.00	88.50	94.30	95.60	95.70	93.10	98.00
BTE	98.40	94.00	91.60	94.00	95.80	95.80	94.00	98.60
RTE	93.30	80.00	66.50	71.80	75.90	79.20	74.40	89.80
Average	94.61	91.53	88.04	88.39	88.89	85.03	85.69	80.05

80% of the dataset (6037 pores and 459 solid matrices) was used for training and 20% for testing

descriptors as shown in Table 1, signifying that the use of more geometrical descriptors might increase the available information and classification accuracy.

In terms of the individual descriptors, the area with an average accuracy of 91.53% for all classifiers had the most significant effect on the microstructural feature description. In addition, circularity performed quite well with most classifiers and had the highest accuracy (98.60%) among individual descriptors with the BTE classifier. However, the least accuracy of 7.90% was observed when circularity was used with the QSVM classifier (Table 1), which led to a reduction in its average classification accuracy (80.05%). Generally, this indicates that the type of classifier used affects the classification accuracy of a given descriptor (Seiffert et al. 2010). Particularly, QSVM is an extension of support vector machine that is specifically designed to separate data nonlinearly (Dagher 2008; Maheshwari et al. 2022). On the other hand, for a single descriptor, the solid matrix can be easily and effectively separated from the pore linearly, since the pore was more circular than the solid matrix (Sect. 4.1). However, QSVM separates the data of individual descriptors nonlinearly, which is hence the possible reason for the relatively lower performance observed with the QSVM classifier for most individual descriptors employed and especially for circularity. In addition, despite not following a specific trend, eccentricity with an average classification accuracy of 85.03% was quite significant. Moreover, other descriptors including centroid, orientation, perimeter and convex area with average classification accuracies of 88.04%, 88.39%, 88.89% and 85.69%, respectively, had a significant effect on classifying the pores and solid matrices (Table 1).

Since the classifiers using all descriptors had the highest average accuracy, a confusion matrix was used to have an in-depth understanding of their discriminative power as presented in Fig. 4. Figure 4a shows the description of the confusion matrix where negative (0) and positive (1) represent the pores and solid matrices, respectively. Although most of the classifiers provided high overall classification accuracy as shown in Table 1, their confusion matrices (Fig. 4b–h) show that most classifiers were biased as a large number of the solid matrices were misclassified due to class imbalance (Kumari and Kr. 2017; Pérez-Ortiz et al. 2016). For FT classifier, false negatives (FN) and false positives (FP) of 18.70%
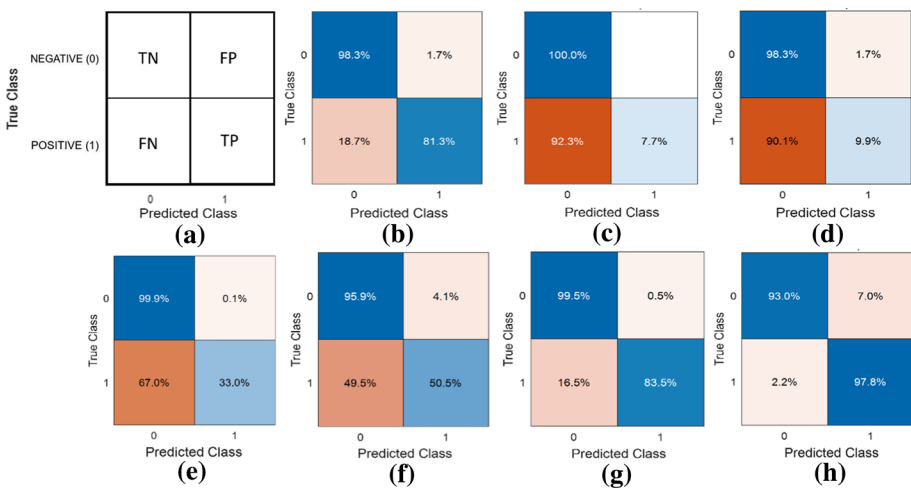
Fig. 4 **a** Confusion matrix description, confusion matrix for **b** FT, **c** LDA, **d** GNB, **e** QSVM, **f** FKNN, **g** BTE, and **h** RTE

and 1.70% were obtained, respectively, as shown in Fig. 4b, implying that 18.70% of all the solid matrices were classified wrongly as pores, while only 1.70% of all the pores were classified wrongly as solid matrices. For LDA classifier, FN of 92.30% was realized as shown in Fig. 4c, meaning that 92.30% of all the solid matrices were wrongly classified, while all the pores were accurately classified. Although with a high accuracy of 93.50% (Table 1), LDA had the highest FN for the solid matrices likely due to its inability to handle the class imbalance between the pores and solid matrices in the bread microstructures (Pérez-Ortiz et al. 2016; Wang et al. 2011).

For GNB classifier, FN and FP of 90.10% and 1.70% were obtained, respectively, as shown in Fig. 4d, implying that 90.10% of all the solid matrices were classified wrongly as pores, while only 1.70% of the pores were classified wrongly as solid matrices. On the other hand, for QSVM classifier, FN and FP of 67.00% and 0.10% were obtained, respectively, as shown in Fig. 4e, meaning that 67.00% of the solid matrices were classified wrongly as pores, while only 0.10% of the pores were classified wrongly as solid matrices. For FKNN classifier, FN and FP of 49.50% and 4.10% for solid matrices and pores were obtained, respectively, as shown in Fig. 4f, implying that 49.50% of all the solid matrices were classified wrongly as pores, while 4.10% of the pores were classified wrongly as solid matrices.

As the best performed classifier, BTE had FN and FP of 16.50% and 0.50% for solid matrices and pores, respectively, as shown in Fig. 4g, implying that 16.50% of all the solid matrices were classified wrongly as pores, while only 0.50% of the pores were classified wrongly as solid matrices. Besides having the highest accuracy (98.40%), BTE had the second least FN for solid matrices, and a very small FP (0.50%) for pores, hence, making it the most suitable classifier for bread microstructural feature classification. For the RTE classifier, FN and FP of 2.20% and 7.00% for solid matrices and pores were obtained, respectively, as shown in Fig. 4h, implying that 2.20% of all the solid matrices were classified wrongly as pores, while 7.00% of pores were classified wrongly as solid matrices. Moreover, RTE had the least FN (2.20%) for solid matrices, and its FP for pores was minimal. Therefore, the ensembles (BTE and RTE) were the best classifiers for classifying between both classes, primarily due to their adaptiveness in handling the problem of class imbalance associated with bread microstructural features (Galar et al. 2012; Kumari and Kr. 2017). Lastly, an increase in the dataset might increase the available information and classification accuracy.

Since the BTE was the most accurate classifier, a "step forward" analysis was used for identifying key descriptors (Pieczywek and Zdunek 2012). In the first step, convex area was excluded and its exclusion had no significant effects on the classifier's accuracy (Table 2). In the next step, the removal of eccentricity led to an increase in the accuracy (Tables 2), implying that it was less significant to the classifier's accuracy. In the third step, the removal of perimeter led to a decrease in accuracy, thus showing that perimeter was significant. Moreover, the highest accuracy of 98.80% was realized using five descriptors (circularity, area, centroid, orientation, and perimeter) as shown in Table 2. Furthermore, these five descriptors had higher classification accuracy than using all descriptors, implying that the addition of more descriptors might not necessarily increase the classification accuracy.

Table 2 Evaluation of key descriptors for feature classification using BTE

Number of descriptors	Descriptors	Accuracy (%)
7	Circularity, area, centroid, orientation, perimeter, eccentricity, and convex area	98.40
6	Circularity, area, centroid, orientation, perimeter, and eccentricity	98.30
5	Circularity, area, centroid, orientation, and perimeter	98.80
4	Circularity, area, centroid, and orientation	98.30
3	Circularity, area, and centroid	97.70
2	Circularity and area	98.50

80% of the dataset (6037 pores and 459 solid matrices) was used for training and 20% for testing

4.3 Validation of Reconstructed Microstructures

Validation using actual microstructure provides a platform for accurate and real comparison with the developed microstructure and is much better than using a standardised microstructure (Rahman et al. 2018c). The randomly selected microstructures were used for validating the reconstructed counterpart. Figure 2 shows the images of the reconstructed microstructures and visual comparison showed that ellipse-fitted microstructures were more similar to the original images than Voronoi-fitted microstructures. This could be attributed to the use of more descriptors for the ellipse reconstruction than for Voronoi reconstruction (Rahman et al. 2018c). Specifically, the ellipse algorithm employed three descriptors (centroid, length of minor axis and major axis) ("Appendix"), while the Voronoi algorithm used only a single descriptor (centroid) for reconstruction. Moreover, in Voronoi-fitted microstructures, virtual equivalents of large pores bounded by small ones could not be generated (Pieczywek et al. 2011). In addition, a statistical comparison of
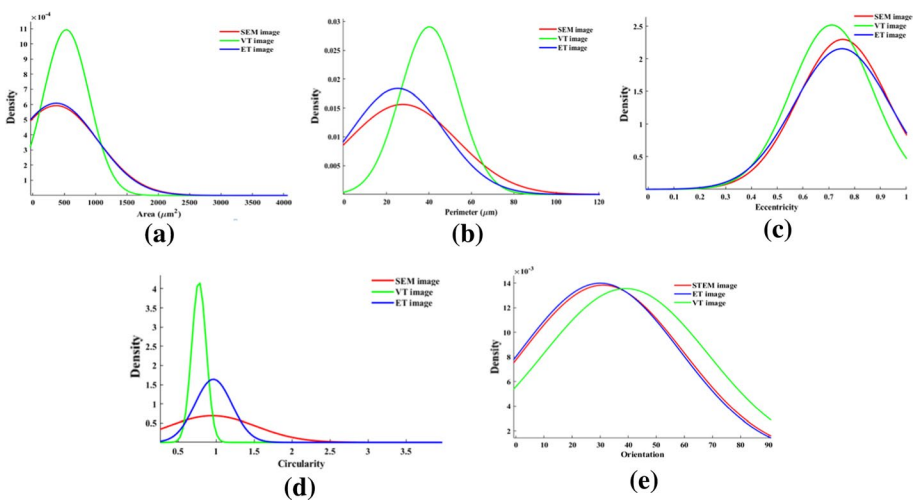
Fig. 5 Comparison of normal distribution between microscopic images, Voronoi and ellipse generated microstructures for sample 1**a** area, **b** perimeter, **c** eccentricity, **d** circularity, **e** orientation
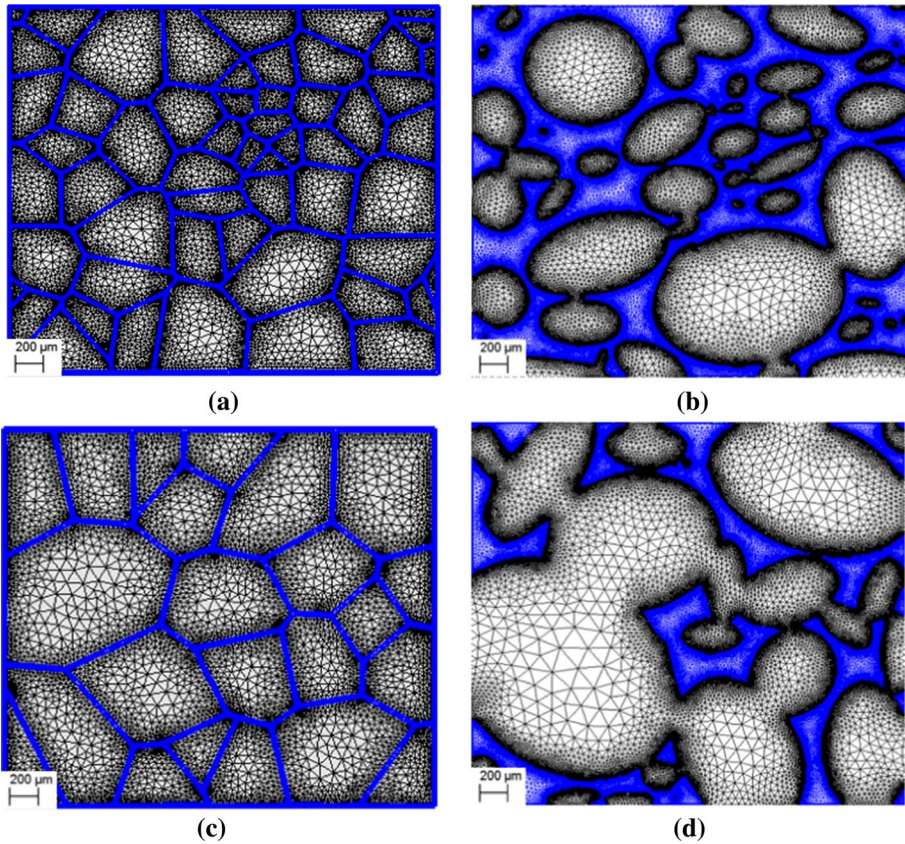
Fig. 6 Sample 1**a** Voronoi generated microstructural mesh, **b** ellipse generated microstructural mesh, sample 2**c** Voronoi generated microstructural mesh, **d** ellipse generated microstructural mesh

the original and reconstructed microstructures was used to investigate the accuracy of the reconstructed microstructures. Figure 5a shows normal distributions of area for the SEM images, Voronoi and ellipse reconstructed microstructures for sample 1, and the distributions of ellipse reconstructed microstructure (p value $= 0.7948$) were in better agreement with those of SEM images than Voronoi reconstructed microstructures (p value $= 1.4554 \times 10^{-5}$). Trends similar to those of area distributions for sample 1 were also observed for the normal distributions of the perimeter, eccentricity, and orientation of sample 1 as shown in Fig. 5b, c, e, respectively, and for all relevant normal distributions for sample 2. However, for both samples, the p value of circularity for the Voronoi reconstructed microstructure was higher than that of the ellipse reconstructed microstructure (Fig. 5d). Furthermore, to reveal the pores/solid matrices connectivity and distribution, meshed computational domains for both samples are shown in Fig. 6, and ellipse generated microstructures provided a better representation of steamed bread microstructures as compared with Voronoi generated microstructure. In addition, pores in ellipse generated microstructures were more open and well connected as depicted by the greyish mesh portions (Fig. 6b,d), compared with those in the Voronoi generated microstructures (Fig. 6a and c), thus, making the former similar to the pores in steamed bread, which are mostly open and interconnected as

observed from micro-tomography experiment (Wang et al. 2011). In addition, the interconnected pores in the ellipse generated microstructures could also allow for accurate prediction of the transport properties during microscale and multiscale modelling. Finally, previous works on the development of fruit microstructures using both algorithms showed that the ellipse tessellation algorithm was superior to the Voronoi tessellation algorithm, which was in line with the current study (Mebatsion et al. 2006a, 2006b; Rahman et al. 2018c).

5 Conclusions

A descriptor-based approach was used for the classification and reconstruction of steamed bread microstructures, and information obtained from the geometrical descriptors was sufficient for describing and reconstructing the pores and solid matrices. For the automatic classification using all descriptors, BTE with overall accuracy of 98.40% had the highest classification accuracy, while Gaussian Naïve Bayes was the least with 92.10% accuracy. In addition, the use of all geometrical descriptors provided better classifications as compared with using a single descriptor. On the other hand, from the step forward analysis, five descriptors namely circularity, area, centroid, orientation, and perimeter had higher overall accuracy than using all descriptors, implying that increase in descriptors might or might not increase the classification accuracy. Moreover, the ensembles (BTE and RTE) were better for classifying bread microstructures since they can handle the problem of class imbalance associated with its microstructural features. In addition, with the automatic classification, large number of images can be processed within a relatively short period of time. Furthermore, evaluating more descriptors beyond those used in the current work could increase information availability and classification accuracy of the microstructural features. Statistical validation of the two approaches with SEM images revealed that the ellipse reconstruction method was more accurate compared to the Voronoi reconstruction method. Also, pictorial evaluation of the reconstructed microstructures in the computational domain showed that the ellipse reconstruction method was more superior in representing the bread microstructural features, the ellipse generated steamed bread microstructures could thus be used as REV for microscale and multiscale numerical modelling of transport phenomena during the processing of steamed bread.

Appendix

MATLAB Code for Ellipse Reconstruction Algorithm

```
function [X,Y] = Ellipse_Fit(s)

for k = 1: length(s) % where s is the total number of all the features of the microstructure (pores and solid matrices)

    a = s(k).MajorAxisLength/2; % length of the major axis of a feature
    b = s(k).MinorAxisLength/2; % length of the minor axis of a feature
```

```
Xc = s(k).Centroid(1); % x coordinate of the ellipse centre
Yc = s(k).Centroid(2); % y coordinate of the ellipse centre
phi = deg2rad(-s(k).Orientation); % angle of rotation in radians with respect to the x-axis
x = Xc + a*cos(t)*cos(phi)—b*sin(t)*sin(phi); % vector representation of an ellipse in
x plane
y = Yc + a*cos(t)*sin(phi) + b*sin(t)*cos(phi); % vector representation of an ellipse in y
plane
plot(x,y,'black','Linewidth',2);


end


end
```

Declarations

Conflict of interest The authors have not disclosed any competing interests.

References

Abera, M.K., Verboven, P., Herremans, E., Defraeye, T., Fanta, S.W., Ho, Q.T., Carmeliet, J., Nicolai, B.M.: 3D virtual pome fruit tissue generation based on cell growth modeling. Food Bioprocess Technol. **7**, 542–555 (2014)

Aguilera, M.: Why food microstructure ? J. Food Eng. **67**, 3–11 (2005)

Aguilera, J.M., Stanley, D.W., Baker, K.W.: New dimensions in microstructure of food products. Trends Food Sci. Technol. **11**, 3–9 (2000)

Ajani, C., Curcio, S., Dejchanchaiwong, R., Tekasakul, P.: Influence of shrinkage during natural rubber sheet drying: numerical modelling of heat and mass transfer. Appl. Therm. Eng. **149**, 798–806 (2019)

Ajani, C.K., Zhu, Z., Sun, D.-W.: Recent advances in multiscale CFD modelling of cooling processes and systems for the agrifood industry. Crit. Rev. Food Sci. Nutr. (2020). https://doi.org/10.1080/10408398.2020.1809992

Altamirano-fortoul, R., Le-bail, A., Chevallier, S., Rosell, C.M.: Effect of the amount of steam during baking on bread crust features and water diffusion. J. Food Eng. **108**(1), 128–134 (2012)

Aregawi, W.A., Abera, M.K., Fanta, S.W., Verboven, P., Nicolai, B.: Prediction of water loss and viscoelastic deformation of apple tissue using a multiscale model. J Phys. Condens. Matter. **26**(46), 464111 (2014)

Brosnan, T., Sun, D.-W.: Evaluation of cut flower vase life by computer vision. Biosyst. Eng. **83**(2), 191–198 (2002)

Chalifour, A., Nouboud, F., Alain, V.: Computation of the area in the discrete plane: Green's theorem revisited. J. Electron. Imaging **26**(6), 1–11 (2017)

Cheng, Q. F., Sun, D.-W.: Effects of combined water cooking-vacuum cooling with water on processing time, mass loss and quality of large pork ham. J. Food Proc. Eng. **30**(1), 51–73 (2007)

Dagher, I.: Quadratic kernel-free non-linear support vector machine. J. Global Optim. **41**(1), 15–30 (2008)

Decost, B.L., Holm, E.A.: A computer vision approach for automated analysis and classification of microstructural image data. Comput. Mater. Sci. **110**, 126–133 (2015)

Derossi, A., Severini, C., Pilli, T.D.: Reconstruction of food microstructure via statistical correlation functions. The use of lineal-path distribution functions. J. Food Eng. **142**, 9–16 (2014)

Derossi, A., Severini, C., Ricci, I.: On the inverse problem of the reconstruction of food microstructure from limited statistical information. A study on bread. J. Food Eng. **184**, 69–74 (2016)

Drummond, L., Sun, D.-W., Vila, C. T.,   Scannell, A. G. M.: Application of immersion vacuum cooling to water-cooked beef joints – quality and safety assessment. LWT - Food Sci. Technol. **42**(1), 332–337 (2009)

Drummond, L., Sun, D.-W.: Evaluation of the immersion vacuum cooling of cooked beef joints – mathematical simulation of variations in beef size and porosity and pressure reduction rates. Innov. Food Sci. Emerg. Technol. **16**, 205–210 (2012)

Esveld, D.C., Van Der Sman, R.G.M., Dalen, G. Van., Van Duynhoven, J.P.M., Meinders, M.B.J.: Effect of morphology on water sorption in cellular solid foods. Part I: pore scale network model. J. Food Eng. **109**(2), 301–310 (2012)

Feng, C.-H., Sun, D.-W.: Optimisation of immersion vacuum cooling operation and quality of irish cooked sausages by using response surface methodology. Int. J. Food Sci. Technol. **49**(8), 1850–1858 (2014)

Galar, M., Fernandez, A., Barrenechea, E., Bustince, H., Herrera, F.: A review on ensembles for the class imbalance problem: bagging-, boosting-, and hybrid-based approaches. IEEE Trans. Syst. Man Cyber Part C (Appl. Rev.) **42**(4), 463–484 (2012). https://doi.org/10.1109/TSMCC.2011.2161285

Gonzales-Barron, U., Butler, F.: Fractal texture analysis of bread crumb digital images. Eur. Food Res. Technol. **226**(4), 721–729 (2008)

Halder, A., Datta, A.K., Spanswick, R.M.: Water transport in cellular tissues during thermal processing. Am. Inst. Chem. Eng. J. **57**(9), 2574–2588 (2011)

Hastie, T., Tibshirani, R., Friedman, J.: The Elements of Statistical Learning, Data Mining, Inference and Pediction, 2nd edn. Springer, New York (2008)

Heertje, I.: Structure and function of food products: a review. Food Struct. **1**(1), 3–23 (2014)

Houska, M., Landfeld, A., Sun, D.-W.: Eating quality enhancement of cooked pork and beef by ripening in brine and vacuum cooling. J. Food Eng. **68**(3), 357–362 (2005)

Kou, X., Luo, D., Zhang, K., Xu, W., Li, X., Xu, B., Li, P., Han, S., Liu, J.: Textural and staling characteristics of steamed bread prepared from soft flour added with inulin. Food Chem. **301**, 125272 (2019)

KumariKr., S., R.: Machine learning: a review on binary classification. Inter. J. Comput. Appli. **160**(7), 11–15 (2017)

Liu, Z., Scanlon, M.G.: Predicting mechanical properties of bread crumb. Food Bioprod. Process. Trans. Inst. Chem. Eng. Part C **81**(3), 224–238 (2003)

Maheshwari, D., Sierra-Sosa, D., Garcia-Zapirain, B.: Variational quantum classifier for binary classification: real versus synthetic dataset. IEEE Access **10**, 3705–3715 (2022)

McClure, J.E., Armstrong, R.T., Berrill, M.A., Schlüter, S., Berg, S., Gray, W.G., Miller, C.T.: Geometric state function for two-fluid flow in porous media. Phys. Rev. Fluids **3**(8), 1–16 (2018)

McDonald, K., Sun, D.-W.: Vacuum cooling technology for the food processing industries: A review. J. Food Eng. **45**(2), 55–65 (2000)

McDonald, K., Sun, D.-W.: Pore size distribution and structure of a cooked beef product as affected by vacuum cooling. J. Food Proc. Eng. **24**(6), 381–403 (2001a)

McDonald, K., Sun, D.-W.: The formation of pores and their effects in a cooked beef product on the efficiency of vacuum cooling. J. Food Eng. **47**(3), 175–183 (2001b)

Mebatsion, H.K., Verboven, P., Verlinden, B.E., Ho, Q.T., Nguyen, T.A., Nicola, B.M.: Microscale modelling of fruit tissue using Voronoi tessellations. Comput. Electron. Agric. **52**, 36–48 (2006a)

Mebatsion, H.K., Verboven, P., Ho, Q.T., Mendoza, F., Verlinden, B.E., Nguyen, T.A., Nicola, B.M.: Modelling fruit microstructure using novel ellipse tessellation algorithm. Comput. Model. Eng. Sci. **14**(1), 1–14 (2006b)

Mulchrone, K.F., Roy, K.: Fitting an ellipse to an arbitrary shape : implications for strain analysis. J. Struct. Geol. **26**, 143–153 (2004)

Ng, H.P., Ong, S.H., Foong, K.W.C., Goh, P.S., & Nowinski, W.L. (2006). Medical image segmentation using k-means clustering and improved watershed algorithm. In: *Proceedings of the IEEE Southwest Symposium on Image Analysis and Interpretation*, pp. 61–65

Novakovic, J., Veljovi, A., Iiic, S., Papic, Z., Tomovic, M.: Evaluation of classification models in machine learning. Theory Appl. Math. Comput. Sci. **7**(1), 39–46 (2017)

Pérez-Ortiz, M., Jiménez-Fernández, S., Gutiérrez, P.A., Alexandre, E., Hervás-Martínez, C., Salcedo-Sanz, S.: A review of classification problems and algorithms in renewable energy applications. Energies **9**(8), 1–27 (2016)

Pieczywek, P.M., Zdunek, A.: Automatic classification of cells and intercellular spaces of apple tissue. Comput. Electron. Agric. **81**, 72–78 (2012)

Pieczywek, P.M., Zdunek, A., Umeda, M.: Study on parameterisation of plant tissue microstructure by confocal microscopy for finite elements modelling. Comput. Electron. Agric. **78**(1), 98–105 (2011)

Prakash, P., Mytri, V.D., Hiremath, P.S.: An improved algorithm for classification of graphite grains in cast iron microstructure. In: Pise, S.J. (ed.) First International Conference on Contours of Computing Technology, pp. 214–218. Springer, New Delhi (2011)

Rahman, M.M., Joardder, M.U.H., Khan, M.I.H., Pham, N.D., Karim, M.A.: Multi-scale model of food drying: current status and challenges. Crit. Rev. Food Sci. Nutr. **58**(5), 858–876 (2018a)

Rahman, M.M., Kumar, C., Joardder, M.U.H., Karim, M.A.: A micro-level transport model for plant-based food materials during drying. Chem. Eng. Sci. **187**, 1–15 (2018b)

Rahman, M.M., Gu, Y.T., Karim, M.A.: Development of realistic food microstructure considering the structural heterogeneity of cells and intercellular space. Food Struct. **15**, 9–16 (2018c)

Richards, J.A., Xiuping, J.: Supervised classification techniques. In Remote sensing digital image analysis. Springer, Heidelberg (2013)

Schröder-Turk, G.E., Mickel, W., Kapfer, S.C., Schaller, F.M., Breidenbach, B., Hug, D., Mecke, K.: Minkowski tensors of anisotropic spatial structure. New J. Phys. **15**, 083028 (2013)

Seiffert, C., Khoshgoftaar, T.M., Van Hulse, J., Napolitano, A.: RUSBoost: a hybrid approach to alleviating class imbalance. IEEE Trans. Syst. Man Cybern. Part A Syst. Hum. **40**(1), 185–197 (2010)

Su, D., Yan, W.M.: Prediction of 3D size and shape descriptors of irregular granular particles from projected 2D images. Acta Geotech. **15**(6), 1533–1555 (2020)

Sun, D.-W., Hu, Z.: CFD simulation of coupled heat and mass transfer through porous foods during vacuum cooling process. Int. J. Refrig. **26**(1), 19-27 (2003)

Sun, D.-W., Wang, L. J.: Development of a mathematical model for vacuum cooling of cooked meats. J. Food Eng. **77**(3), 379-385 (2006)

Sundararaghavan, V., Zabaras, N.: Classification and reconstruction of three-dimensional microstructures using support vector machines. Comput. Mater. Sci. **32**, 223–239 (2005)

Tharwat, A., Gaber, T., Ibrahim, A., Hassanien, A.E.: Linear discriminant analysis: a detailed tutorial. AI Commun. **30**(2), 169–190 (2017)

Thomas, M., Boyard, N., Perez, L., Jarny, Y., Delaunay, D.: Representative volume element of anisotropic unidirectional carbon–epoxy composite with high-fibre volume fraction. Compos. Sci. Technol. **68**(15–16), 3184–3192 (2008)

Wang, S., Austin, P., Bell, S.: It's a maze: the pore structure of bread crumbs. J. Cereal Sci. **54**(2), 203–210 (2011)

Wang. L. J., Sun, D.-W.: Modelling vacuum cooling process of cooked meat, part 1 - analysis of vacuum cooling system. Int. J. Refrig. **25**(7), 854–861 (2002a)

Wang. L. J., Sun, D.-W.: Modelling vacuum cooling process of cooked meat, part 2 - mass and heat transfer of cooked meat under vacuum pressure. Int. J. Refrig. **25**(7), 862–871 (2002b)

Wang. L. J., Sun, D.-W.: Numerical analysis of the three dimensional mass and heat transfer with inner moisture evaporation in porous cooked meat joints during vacuum cooling process. Trans. ASAE **46**(1), 107-115 (2003)

Xu, H., Li, Y., Brinson, C., Chen, W.: A descriptor-based design methodology for developing heterogeneous microstructural materials system. J. Mech. Des. **136**, 1–12 (2014b)

Xu, H., Ruoqian, L., Alok, C., Wei, C.: A machine learning-based design representation method for designing heterogeneous microstructures. In: *Proceedings of the ASME 2014a International Design Engineering Technical Conferences and Computers and Information in Engineering Conference*, pp. 1–12 (2014a)

Zhang, Z. H., Sun, D.-W.: Modelling of three-dimensional heat and mass transfer during vacuum cooling of cooked diced beefs. Acta Horticult. **674**, 199-204 (2005)

Zhang, Z., Drummond, L., D.-W.: Vacuum cooling in bulk of beef pieces of different sizes and shape - evaluation and comparison to conventional cooling methods. J. Food Eng. **116**(2), 581–587 (2013)